CHARACTERIZATION OF THE FIBROUS MICROSTRUCTURE OF SMC DURING COMPRESSION MOULDING USING X-RAY MICROTOMOGRAPHY

Thai-Hung Le*, Pierre Dumont**, Laurent Orgéas*, Denis Favier*, Luc Salvo***, Elodie Boller**** [Pierre Dumont]: pierre.dumont@efpg.inpg.fr
*Laboratoire Sols-Solides-Structures (3S), CNRS – Universités de Grenoble, BP 53, 38041 Grenoble cedex 9 France,
**Laboratoire de Génie des Procédés Papetiers (LGP2), CNRS-INPG-EFPG, BP 65, 461, rue de la Papeterie, 38402 Saint-Martin-d'Hères cedex, France
***Laboratoire de Génie Physique et Mécanique des Matériaux (GPM2), CNRS-INPG, 101, rue de la Physique, 38402 Saint-Martin-d'Hères cedex, France,
****European Synchrotron Radiation Facility (ESRF), ID19 Topography & Microtomography Group, 6, rue Jules Horowitz, BP 220, 38043 Grenoble cedex, France

Keywords: *SMC, porosity, segregation, bundle-microstructure, bundle-orientation, microtomography, phase contrast.*

Abstract

The X-ray microtomography technique was used to analyze the porosity of the fiber bundle distribution of sheet molding compounds (SMC) samples taken from non-deformed and deformed plates. For that purpose, the phase contrast imaging mode was shown to be the most effective. A large decrease of the porosity after molding is observed, this phenomenon being enhanced for preheated plates. Analysis of the fiber fraction distribution reveals that a segregation phenomenon between fiber-bundles and the polymer matrix occurs through the thickness of SMC during molding.

1 Introduction

The Sheet Molding Compounds (SMC) are widely used by the car industry to produce cost-efficient lightweight and large body panels. SMC form continuous sheets (thickness $\approx$ 2–3 mm) containing $\approx$ 25 wt% chopped glass fiber-bundle mats (length $\approx$ 10–50 mm, averaged diameter $\approx$ 0.05–1 mm) embedded in a thermoset pasty matrix essentially made of $CaCO_3$ ($\approx$ 45 wt%), polyester resin ($\approx$ 25 wt%) and other products ($\approx$ 5 wt%). At ambient temperature, SMC sheets are cut, stacked and placed in a hot mould ($\approx$ 150°C). Then, they are squeezed at a closure velocity of $\approx$ 0.1–10 mm s^{-1}. Once the mould is filled, it is maintained close during the curing stage ($\approx$ 60–120 s). Finally the molded part is ejected. The flow stage has a major influence on the final properties of produced parts. Although flow mechanisms of SMC materials are quite well described at the macroscopic scale [1-2], it remains difficult to characterize finely and easily the flow-induced fibrous microstructures during the compression stage by using usual techniques such as burning and weighting techniques, microscopy, X-ray radiography… One of the hindering points is the poor contrast between the physical properties of the polymer matrix, which contains a large amount of $CaCO_3$ fillers, and the glass fiber-bundles. This makes difficult to discuss or to improve the validity of the physical assumptions usually stated at the bundle scale in order to develop rheological models designed for predicting the flow and the evolution of the microstructure of SMC [3-7]. Consequently, various important questions are still opened: How do the porosity and the fiber content evolve during the flow stage? In this study, the X-ray microtomography imaging technique was used to estimate the benefits, which can be expected to answer such questions.

2 Experiments

The SMC that were compression molded in [8] were standard Low Profile SMC (LP 606) processed by Mecelec Composite and Recyclage (Tournon, France). The initial sheets having an average thickness of approximately 2.5 mm were composed of a polyester resin that was mainly filled with $CaCO_3$ mineral charges of typical diameter 2 μm and glass fiber-bundles ($\approx$ 25 wt%), with

approximately elliptical cross section (major axis $a_{00} \approx 0.66$ mm and minor axis $b_{00} \approx 0.06$ mm), each of them containing 200 fibers of diameter d = 15 μm and length l = 25 mm.

Compression molding experiments were performed using an instrumented industrial hydraulic press (maximum axial force of 4000 kN and axial maximum velocity 40 mm s^{-1}, Compositec, Chambéry, France). This press was equipped with a standard mould used to produce square plates of constant thickness, which could be modified by adding an aluminum stair part to produce square plates with a variable thickness (in-plane dimensions of 500×500 mm^2). For all moldings, the mould temperature was maintained constant at 150°C and the initial surface of all SMC charges put inside the moulds was $S_0 = l_0 \times L_0 = 170 \times 500$ mm^2.

The microstructures of four plates of the previous study have been characterized here, all the considered plates being compressed with an axial punch velocity of 1 mm s^{-1} and with an initial charge put in the left part of the mould, see figure 1. Moreover, the maximum limit of the axial compression force was fixed to 2500 kN, leading to an average mould closing pressure p of 10 MPa.

The first plate, i.e. plate A (cf. figure 1a), was obtained without material flow, i.e. just by curing by simple contact with the upper and lower parts of the mould a SMC charge made of five SMC stacked layers (initially at room temperature, i.e. 30°C).

The second plate, i.e. plate B (figure 1b), was molded in the standard mould from an initial SMC charge made of three stacked layers preheated at 60°C for 10 min.
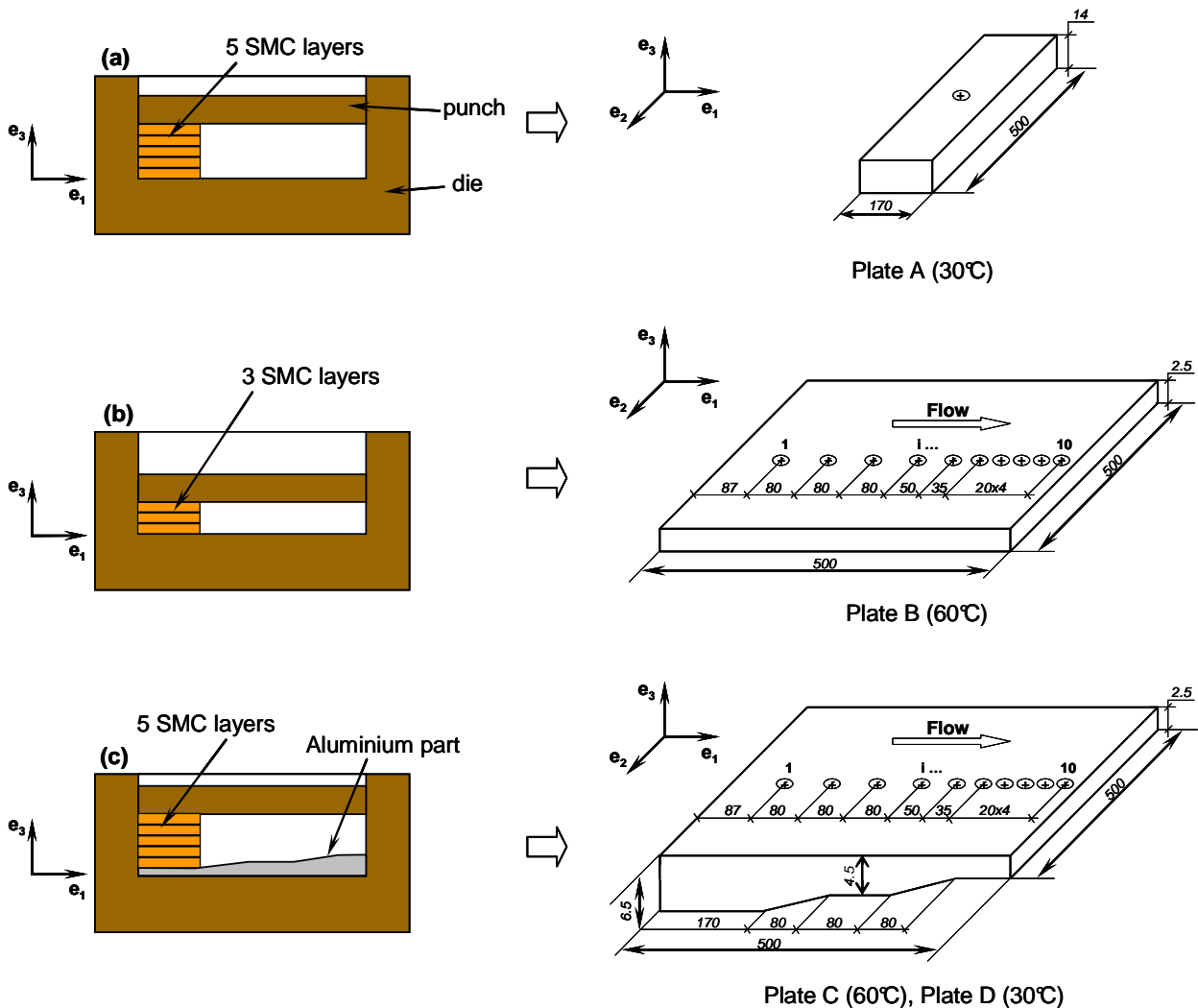

Fig. 1. Schematic representations of the side views of the standard and modified moulds with the initial charges of SMC (left) used to produce plates A (a), B (b) and C,D (c) (right). Circles drawn on the surfaces of the compression molded plates indicate the location of cylindrical samples that were cut and used for X-ray microtomography.

Two last plates, i.e. plates C and D (figure 1c), were molded in the modified mould from an initial stack of five SMC layers. Among these two plates, plate C was initially preheated at 60°C for 10 min and plate D was obtained from a SMC charge initially at room temperature.

3 X-ray microtomography

In order to obtain 3D representations of the SMC microstructures with X-ray microtomography, cylindrical samples (height 2 mm $<h<$14 mm and diameter d=10 mm) were first cut using a water-jet cutting machine in different locations of the produced plates A, B, C and D. Circles drawn on the surface of the plates of the right-hand side of figure 1 indicate the locations of these samples. For the non-deformed plate A, only one sample was cut in the middle of the plate. For the other plates, ten cylindrical samples were cut along a line parallel to the flow direction. For instance, for plate B, these samples were named B_1, … , B_i, …, B_{10} with the index i increasing as the samples were closer to the flow front.

The cut samples were then scanned using the X-ray source provided at the European Synchrotron Radiation Facility (ESRF) on beamline ID19. More precisely, they were exposed to an electron beam energy of 35 keV as a 2048×2048 CCD camera (Frelon, ESRF) took pictures of 1500 projections over 180 degrees of the cylindrical samples. Typically the time needed to scan completely a sample was about 6 min. From these projections, a specially designed software (ESRF) was used to reconstruct 3D grey scale images (256 grey levels) of the scanned samples with a voxel size of 7.5 mm.

Due to the weak difference between the absorption properties of the glass fiber-bundles and the filled polyester matrix, it is difficult to characterize the SMC microstructures from usual absorption mode microtomography [9]. Hence, to enhance the contrast between the SMC matrix and the bundles and to obtain pictures like in figure 1, the phase contrast mode microtomography was used [10].

In order to gain estimates of the volume fractions of pores and bundles, the 3D grey scale images were first ``cleaned'' with a standard 3D median filter in order to reduce the random noise (by using the software ImageJ). Therewith, in order to extract the pores or the fiber-bundle networks from the SMC, scanned volumes were then subjected (ImageJ) to a grey scale thresholding followed by a binarisation. As shown in figure 2, these operations allow obtaining 3D binary renderings of the porosity as well as the bundle networks. They also permit to get an estimation of the porosity (and the volume fraction of fibres), defined as the ratio [number of white voxels]/[total number of voxels] within a given volume. Hence, two main different measurements of volume fractions will be used in the following: (i) ϕ and f, respectively defined as the volume fractions of pores and fibers in a given stack of horizontal voxels, i.e. voxels lying in a given plane parallel to (e_1, e_2), and (ii) $<\phi>$ and $<f>$ respectively defined as the average volume fractions of pores and fibers in a whole analyzed sample.

It is important to notice that due to the rather important voxel size used for the present measurements (7.5 mm), it has not been possible to capture micropores, e.g. some of the pores that may have been contained inside the bundles. Therefore the estimation of the porosity given in the following only concerns mesopores, i.e. pores, which minimum size is of the order of the voxel size. Similarly, the determined volume fraction of fibers must be seen as a first rough estimation of the actual fiber content, since the 7.5 mm size of voxels cannot properly describe fibers which diameters equal 15 mm. Scans performed with a lower voxel size, e.g. 0.7 mm, would surely give better estimates of the pore and fiber contents. However, such scans would require a much smaller sample size, e.g. 1.4 mm, from which the bundle geometry would not be accessible.

The grey scale thresholding carried out to extract mesopores from the SMC did not present major difficulties. A scattering of approx. ± 0.001 was observed for the determined values of ϕ and $<\phi>$. By contrast, the grey scale thresholding, which was required to extract fiber-bundles from the matrix, was much trickier to achieve, even with volumes obtained using the phase contrast mode. It can be shown experimentally that the absolute volume fraction of fibers f and of the relative volume fraction of fibers $\Delta f = f\text{-}<f>$, both being estimated with the three above threshold values, that within the admissible range of threshold values, very poor estimations of the absolute fiber contents f and $<f>$ can be obtained, i.e. with a scattering of ± 0.07. Nonetheless much better results can be gained with the relative fiber content Δf, i.e. with a scattering of ±0.01.

Thai-Hung Le, P. Dumont, L. Orgéas, D. Favier, L. Salvo, E. Boller

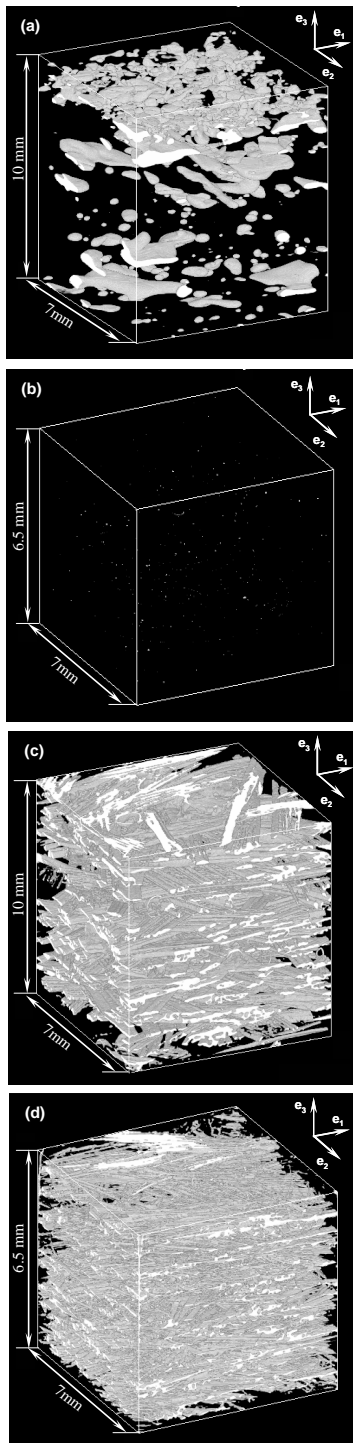

Fig. 2. 3D micrographs taken from samples A (a,c, non-deformed sample, 0 mm < x3 < 10 mm) and C2 (b,d, after compression molding, 0 mm < x3 < 6.5 mm), showing the pores (a,b) and the bundles (c,d). They have been obtained by X-ray microtomography with the phase contrast mode, followed by a filtering, a thresholding and a binarisation.

4 Analysis of volume fractions of fibers and porosity through the thickness and along the produced parts

Figure 3a and b show the evolutions of the volume fraction of fibers f and the porosity ϕ through the thickness of the non-deformed sample A. Figures 3c-e give the variation of the fiber volume fraction f through the thicknesses of all scanned deformed samples B_i, C_i and D_i.

The evolution of the average volume fraction of fibers $<f>$ along the length x_1 of molded plates B, C and D is given in figure 4. Lastly, a typical evolution of the porosity through the thickness of the deformed samples is illustrated in figure 5a in case of the sample C_2, whereas figure 5b shows the profile of the average porosity $<\phi>$ along the length x_1 of plates B, C and D. These four figures bring up the following remarks for the non-deformed and deformed samples.

4.1 Non-deformed sample

As seen from figure 3a, a ``crenellated" profile of the fiber content f is observed in the non-deformed sample A. Zones where f attains its minimum values correspond to the interfaces between the five SMC layers of the initial stack used for this molding, see figure 1a. These interfaces are indicated by dashed-dotted lines in figure 3a.

Inside each layer, there is a systematic microstructure made of upper and lower skins, in which f is much lower than in a core zone, where f is roughly constant. Such a fiber content profile is induced during processing of SMC layers, i.e. during impregnation of fiber-bundle mats by the polymer matrix. The thicknesses e+, e- and e_c of the upper "+" and lower "-" skins "s" as well as the core "c" zone have been estimated, see figure 3a, in the five layers, respectively. In average, e+ ≈ 0.27 mm is very close to e- ≈ 0.28 mm. The corresponding average fiber contents $<f^+_s>$, $<f^-_s>$ and $<f_c>$ have been determined. The average value of the fiber content in the skins approaches 12 %; that in the core zones 21.5%.

Notice that the estimated average fiber content in the layers is 18.8%. Hence, despite the difficulties encountered to get an accurate estimate of the fiber content from the X-ray microtomographs (cf. previous subsection), this value is fairly close to the value of 17.4 % ± 1 % obtained previously on the same SMC with a charring-weighting technique [8].

The average porosity $<\phi>$ in the non-deformed sample A is approximately 6.4 %. It is consistent

with that estimated on a non-cured industrial SMC by [9], using X-ray microtomography and resin infiltration. The dashed-dotted lines delimiting the interfaces between stacked layers have also been drawn in figure 3b. Around these interfaces, the porosity is found to be higher than in the core of the layers, except for the upper layer 5. In that layer, the average porosity $<\phi_l>$ equals 25 % whereas $<\phi_l>$ is smaller in the other layers. Such a higher pore

content is also visually confirmed on the 3D microtomograph shown in figure 2a. It is probably induced by the heating of the samples and may be correlated to thermally activated coalescence and rising motion, before complete cross-linking of the polyester resin, of gaseous components of SMC, such as entrapped air and boiling styrene bubbles [2].
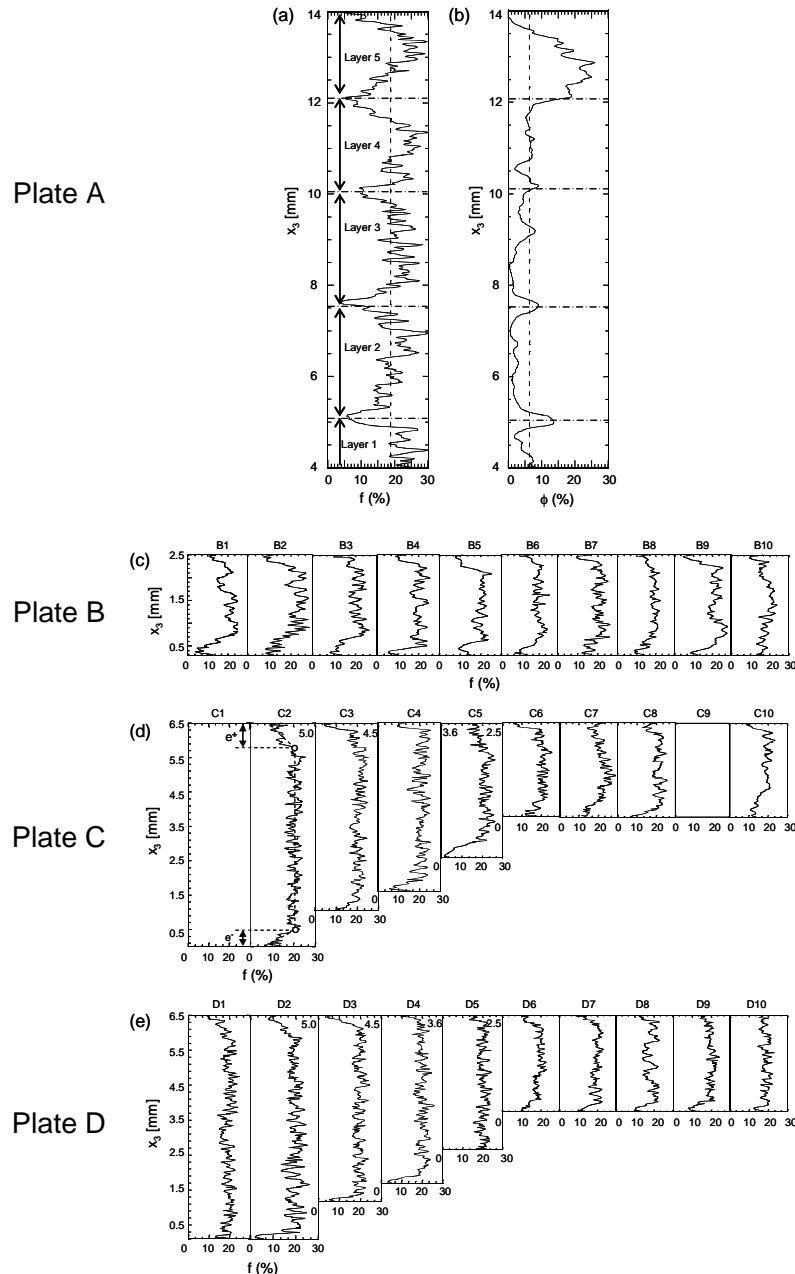

Fig. 3. Evolution (a) of the fiber volume fraction f and (b) of the porosity φ through the thickness x3 of the non-deformed sample A. Evolution of the fiber volume fraction through the thickness x3 of the samples cut from plates B (c), C (d) and D (e).

4.2 Deformed samples

As shown from figure 3, there is a strong contrast between the profile of the volume fraction of fibers f in the non-deformed sample A and those measured in the deformed samples B_i, C_i and D_i:
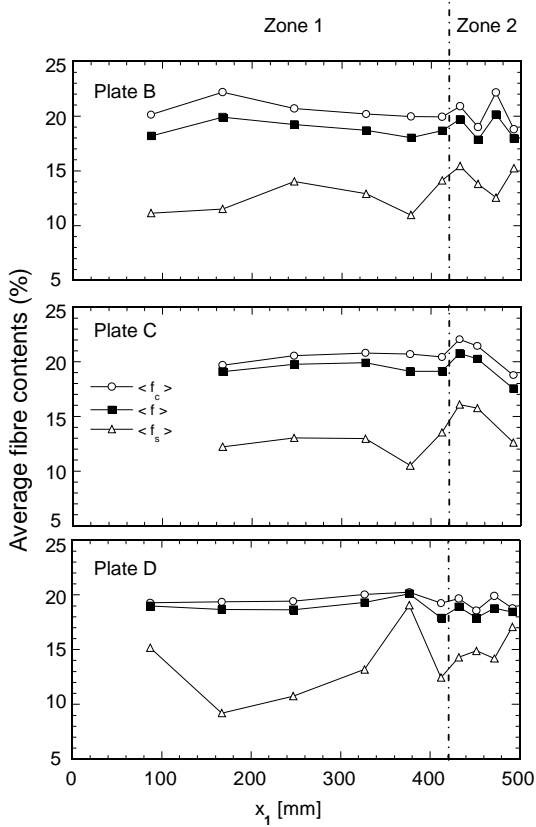

Fig. 4. Evolution of the average values of the fiber contents $<f_c>$, $<f_s>$, $<f>$ along the flow direction x_1 of compression molded plates B, C and D.

- The interfaces between the initial SMC layers have disappeared. The microstructures of the whole deformed samples reduce to core zones, in which the fiber content is high and fairly constant ($f \geq 20$ %), and to upper and lower skins near the interfaces between the mould and the samples, where the fiber content is much lower. This observation suggests that a segregation phenomenon occurs between the fiber-bundles and the polymer matrix during flow through the thickness of SMC. The thicknesses $e+$ and $e-$ of the upper and lower skins of the deformed samples have been measured, as shown for sample C_2 in figure 3d. Whatever the molding conditions, the initial SMC temperatures, the sample location, and

even if the lower skins were in contact with the hot mold surface for approximately 10 s before flowing, $e+$ and $e-$ are both very close and equal in average to 0.22 mm and 0.26 mm, respectively.
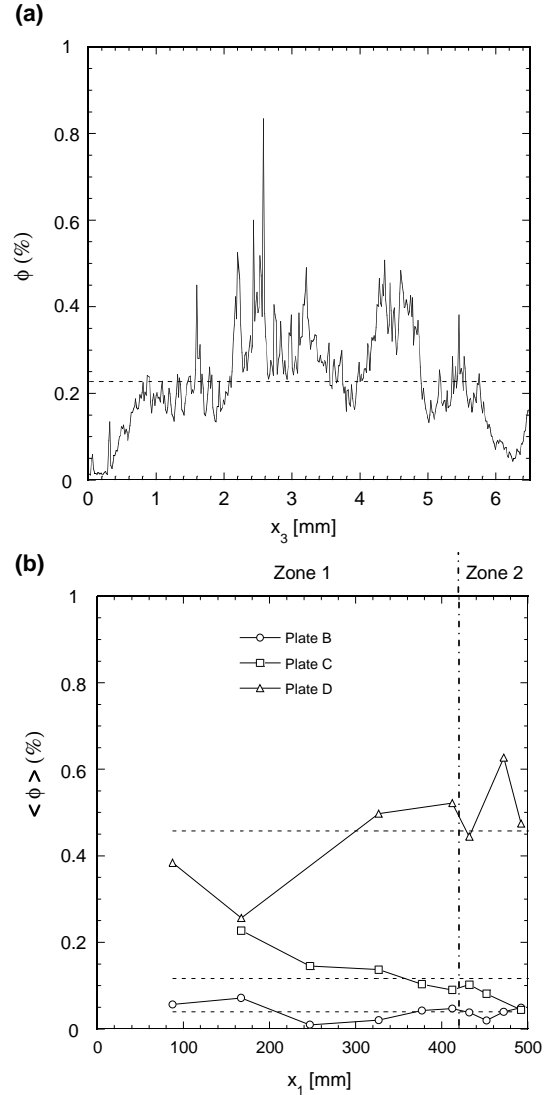

Fig. 5. Evolution (a) of the porosity φ through the thickness x_3 of the deformed sample C_2 and (b) of the average porosity $<\phi>$ along the flow direction x_1 of compression molded plates B, C and D.

- Moreover, figure 4 shows that in a first zone (Zone 1) corresponding approximately to $0<x_1<420$ mm, the average fiber contents in the skins, the core zone and the samples, i.e. $<f_c>$ and $<f>$, are almost constant. Behind the flow front (Zone 2, 420 mm$<x_1<$500 mm), some irregular and weak variations are observed. Similar conclusions were drawn previously, by

measuring the fiber content with a charring-weighting technique [8].

- A typical porosity profile in the thickness of the deformed samples is given in figure 5a (sample C_2). It is very different from the profile recorded for the non-deformed sample *A*: it exhibits a skin-core-skin sub-structure with higher pore content in the core zone than in skins. As evident from the micrographs shown in figures 2a-b and by comparing figures 2b and 5a, pores in the deformed sample C_2 are much smaller and less dense than those contained in the non-deformed sample *A*.

- Figure 5b proves that the last observation holds for all scanned samples and whatever the molding conditions: $<\phi> \approx 0.04$ % for plate *B*, $<\phi> \approx 0.12$ % for plate *C* and $<\phi> \approx 0.46$ % for plate *D*, whereas $<\phi> \approx 6.4$ % for plate *A*. This figure also illustrates (i) the influence of the mold type, e.g. $<\phi>$ is slightly higher for the stair plate *C* than for the plane plate *B*, and (ii) the influence of the initial temperature of the SMC charges, e.g. $<\phi>$ is lower for the preheated plate *C* than for the plate *D*, initially at room temperature.

5 Conclusion

The X-ray microtomography using the phase contrast mode permits to study some mechanisms of the evolution of the SMC microstructure parameters, such as the porosity, the volume fraction of fibers. The different observations that permit this tool can be useful to improve mesocopic flow models of SMC materials.

These results might be completed by analyzing more finely the fibrous microstructure (flattening and widening of bundles).

References

[1] Barone M, Caulk D., "Kinematics of flow in sheet molding compound", *Polym. Compos.* Vol. 6, pp. 105–109, 1985.

[2] Odenberger P, Andersson H, Lundström T., "Experimental flow-front visualisation in compression moulding of SMC", *Composites Part A,* Vol. 35, pp. 1125–1134, 2004.

[3] Souloumiac B. and M. Vincent, "Steady shear viscosity of short fibre suspensions in thermoplastics", *Rheol. Acta*, Vol. 37, pp. 289, 1998.

[4] Sundararajakumar R. R. and D. L. Koch, "Structure and properties of sheared fiber suspensions with mechanical contacts", *J. Non-Newtonian Fluid Mech.*, Vol. 73, pp. 205, 1997.

[5] Fan X., N. Phan-Thien and R. Zheng, "A direct simulation of fibre suspensions", *J. Non-Newtonian Fluid Mech.*, Vol. 74, pp. 113, 1998.

[6] Toll S., and J.-A. E. Månson, "Dynamics of a planar concentrated suspension with non-hydrodynamic interaction", *J. Rheol.*, Vol. 38, No. 4, pp. 985, 1994.

[7] Le Corre S, Dumont P, Orgéas L, Favier D., "Rheology of highly concentrated planar fiber suspensions", *J Rheol.*, Vol. 49, pp.1029–1058, 2005.

[8] Dumont P, Orgéas L, Favier D, Pizette P, Venet C, "Compression moulding of SMC: In situ experiments, modelling and simulation", *Composites Part A,* Vol. 38, pp. 353-368, 2007.

[9] Comte, E., Merhi, D., Michaud, V., Månson, J.-A.E., "Void formation and transport during SMC manufacturing: effect of the glass fiber sizing", *Polym. Compos.*, Vol. 27, pp. 289-298, 2006.

[10] Cloetens, P., Pateyron-Salomé, M., Buffière, J.-Y., Peix, G., Baruchel, J., Peyrin, F. & Schlenker, M., "Observation of microstructure and damage in materials by phase sensitive radiography and tomography", *J. Appl. Phys.*, Vol. 91, pp. 5878-5886, 1997.